Volume 17 | Number 34 | 14 September 2019 | Pages 7797–8020

Organic & Biomolecular Chemistry

rsc.li/obc

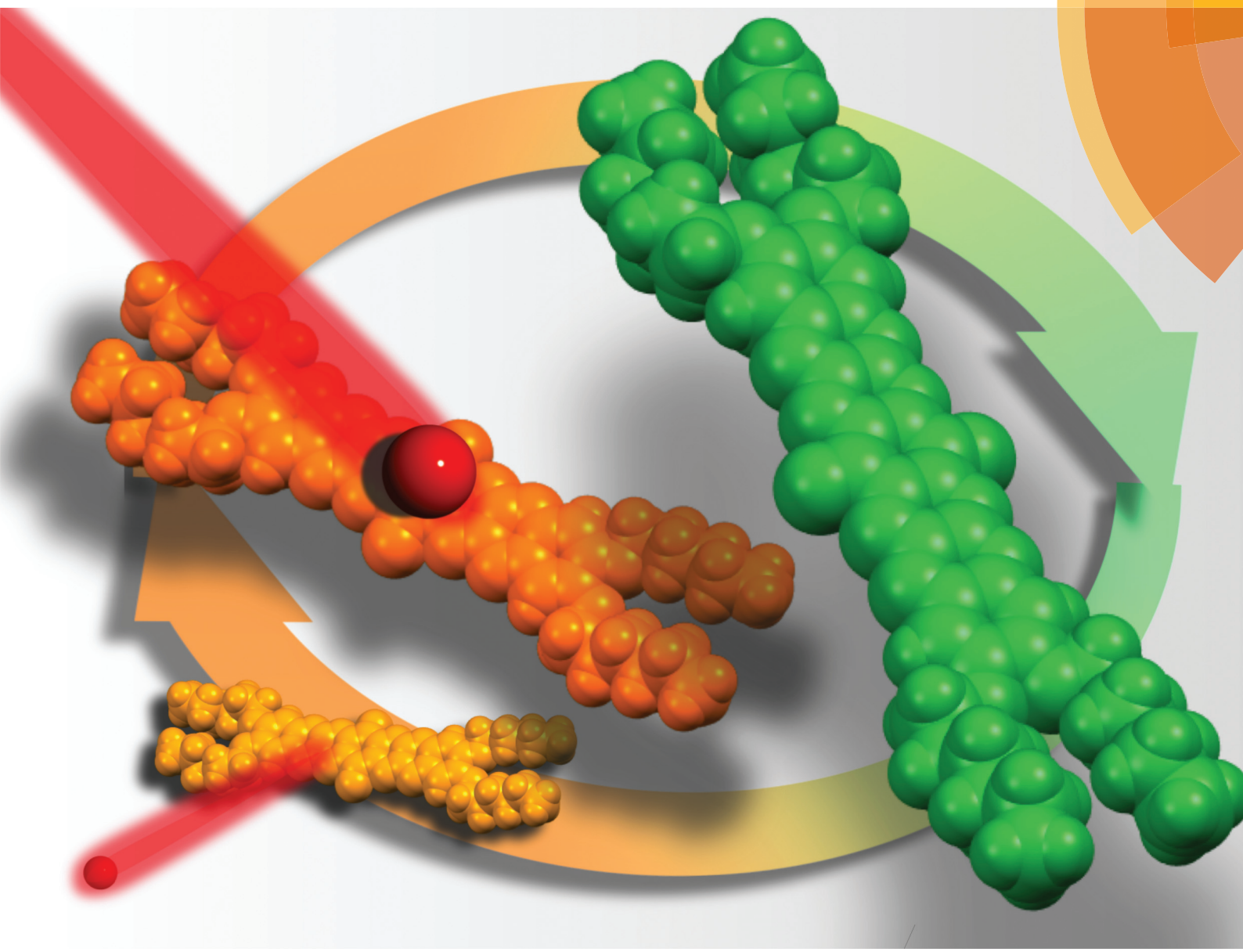

ISSN 1477-0520

ROYAL SOCIETY OF CHEMISTRY | Celebrating IYPT 2019

PAPER
Kyosuke Isoda, Makoto Tadokoro *et al.*
Synthesis and electrochromic behavior of a multi-electron redox-active N-heteroheptacenequinone

Organic & Biomolecular Chemistry

PAPER

Cite this: *Org. Biomol. Chem.*, 2019, **17**, 7884

Synthesis and electrochromic behavior of a multi-electron redox-active N-heteroheptacenequinone†

Kyosuke Isoda, *[a,b] Mitsuru Matsuzaka,[a] Tomoaki Sugaya, [a,c] Takeshi Yasuda[d] and Makoto Tadokoro *[a]

Received 10th June 2019,
Accepted 2nd July 2019

DOI: 10.1039/c9ob01323g

rsc.li/obc

We report a novel N-heteroheptacenequinone derivative (**C_6OAHCQ**) as a large π-conjugated framework. **C_6OAHCQ** shows good electron-accepting behaviour owing to eight electron-deficient imino-N atoms and two carbonyl moieties and excellent solubility in common organic solvents. When a potential between 0 and −2.20 V is applied, **C_6OAHCQ** is able to accept four electrons, which is more than fullerene C_{60} (three electrons) could accept in this voltage range. Moreover, a solution of **C_6OAHCQ** and $^{n}Bu_4NPF_6$ in CH_2Cl_2 exhibits a clearly reversible brown-to-green colour change, suggesting that **C_6OAHCQ** has potential as an electrochromic material.

Introduction

The introduction of heteroatoms into polycyclic aromatic hydrocarbons (PAHs) has been investigated because novel heteroacenes exhibit different electronic and physical properties to PAH molecules and the molecules in their crystal structures are also packed differently to PAHs.[1–7] Among them, we focused on N-heteroacenes in which some of the carbon atoms in PAHs are replaced with nitrogen atoms.[8–19] The development of N-heteroacenes based on the oxidised form is necessary in order to expand the series of electron-accepting frameworks. Novel N-heteroacene-based π-conjugated frameworks have been designed and modified by increasing the number of linearly fused rings and by introducing a variety of substituents. The former approach is essential in order to raise HOMO and lower LUMO levels, leading to π-conjugated molecules with low energy band gaps. However, there are some drawbacks associated with this approach, since some N-heteroacenes are unstable in air and UV-vis light and are insoluble in organic solvents.[20–25] On the other hand, the introduction of a pyrazine framework comprising two imino-N atoms in the latter approach is a simple method for improving the electron-accepting properties without changing the fundamental planar shape of the π-conjugated framework.[11,14] Moreover, both experimental studies and quantum-chemical calculations suggest that the LUMO level is stabilised by increasing the number of imino-N atoms in the π-conjugated framework.[24,26,27] However, oxidation from the reduced form to the oxidised form becomes more difficult with the increasing numbers of hydro-N atoms in the framework. To improve the electron-accepting properties, we designed N-heteroacene molecules based on the benzoquinone framework.

Benzoquinone derivatives function as electron acceptors because of their two electron-withdrawing carbonyl groups. Since benzoquinone derivatives behave as organic oxidising agents in organic syntheses and biological systems, the introduction of this framework will effectively improve the electron-accepting properties of the molecule.[28–31] A benzoquinone-based N-heteroacene (N-heteroquinone) is composed of both benzoquinone and pyrazine units.[32–36] Among them, tetraazapentacenequinone (**TAPQ**) derivatives are products from the oxidation of homofluoridine and are also useful precursors for the preparation of the corresponding N-heteroazaacenes and triisopropylsilyl-appended derivatives.[20,36] Recently, Miao and co-workers reported a simple synthetic route to N-pentacenequinones composed of five linearly fused rings that serve as electron acceptors and *n*-type organic semiconductors.[32–36] Moreover, the electronic properties and the molecular packing in the crystal state can be tuned by changing the positions of the imino-N atoms in **TAPQ**. As mentioned above, further modifications are very important for the development of novel electron-accepting functional frameworks based on N-heteroacenequinone. Herein, we report on the synthesis of an N-heteroheptacenequinone derivative

[a]*Department of Chemistry, Faculty of Science, Tokyo University of Science, 1-3 Kagurazaka, Shinjuku-ku, Tokyo 162-8601, Japan. E-mail: tadokoro@rs.kagu.tus.ac.jp*
[b]*Faculty of Engineering and Design, Kagawa University, 2217-20 Hayashi-cho, Takamatsu, Kagawa 761-0396, Japan. E-mail: k-isoda@eng.kagawa-u.ac.jp*
[c]*Education Center, Faculty of Engineering, Chiba Institute of Technology, 2-1-1 Shibazono, Narashino, Chiba 275-0023, Japan*
[d]*Research Center for Functional Materials, National Institute for Materials Science (NIMS), 1-2-1 Sengene, Tsukuba, Ibaraki 305-0047, Japan*

†Electronic supplementary information (ESI) available. CCDC 1871181. For ESI and crystallographic data in CIF or other electronic format see DOI: 10.1039/c9ob01323g

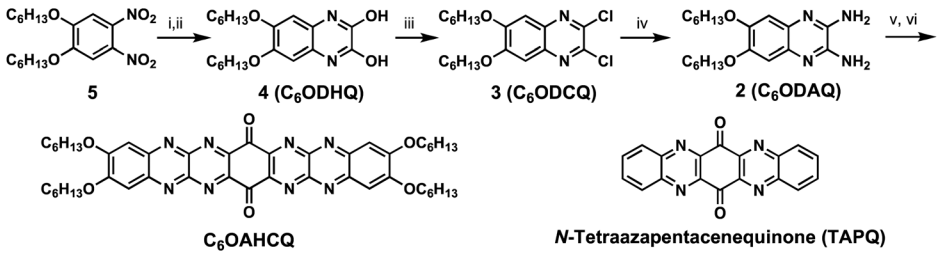

Scheme 1 Synthesis of **C_6OAHCQ** and N-tetraazapentacenequinone (**TAPQ**) as a reference. (i) $N_2H_4{\cdot}H_2O$ and Pd/C in EtOH; (ii) diethyl oxalate in EtOH, 71.2%; (iii) $POCl_3$ in DMA, 91.0%; (iv) liquid NH_3, quantitative; (v) 5,6-dihydroxy-5-cuclohexene-1,2,3,4-tetrone-dihydrate in AcOH; and (vi) $NaIO_4$ and TBAB in CH_2Cl_2/H_2O, 72.1%.

(**C_6OAHCQ**) composed of eight oxidised imino-N atoms (Scheme 1). **OAHCQ** is very stable in air and UV-vis light in the solid state, and it is very soluble in general organic solvents when appropriate flexible alkoxy-chain substituents are included on its terminal benzene rings. Moreover, the **OAHCQ** derivative exhibits electrochromic behaviour because of the redox stability arising from its expanded fused-ring structure.

Results and discussion

Molecular design and synthesis

C_6OAHCQ, bearing four alkoxy chains, was prepared in high yield through a four-step reaction sequence (Scheme 1). 4,5-Dihexyloxy-1,2-dinitrobenzene (**5**)[37] was treated with $N_2H_4{\cdot}H_2O$ and 10% Pd/C in dry EtOH under an Ar atmosphere to give the corresponding reduced dialkoxyphenylene diamine, which was then reacted with diethyl oxalate in dry EtOH to afford pyrazine **4** in 71% yield. Dichloropyrazine **3** was obtained in 91% yield by the reaction of **4** with $POCl_3$ in dimethylaniline (DMA). The treatment of **3** with liquid ammonia in an autoclave for one week afforded diaminopyrazine **2** in quantitative yield; **2** was then reacted with 5,6-dihydroxy-5-cyclohexene-1,2,3,4-tetrone dihydrate in dry acetic acid, followed by $NaIO_4$ and tetrabutylammonium bromide (TBAB) in CH_2Cl_2 to afford **C_6OAHCQ** in 72% yield.[38] The introduction of four flexible alkoxy chains onto the large π-conjugated framework engenders **C_6OAHCQ** with high solubility in common organic solvents, such as $CHCl_3$, CH_2Cl_2, and EtOAc.

Molecular packing and DFT calculations

A single crystal of **C_6OAHCQ** was grown from a solution of DMSO. As shown in Fig. 1, the single-crystal X-ray analysis of **C_6OAHCQ·(DMSO)** reveals that the π-conjugated framework

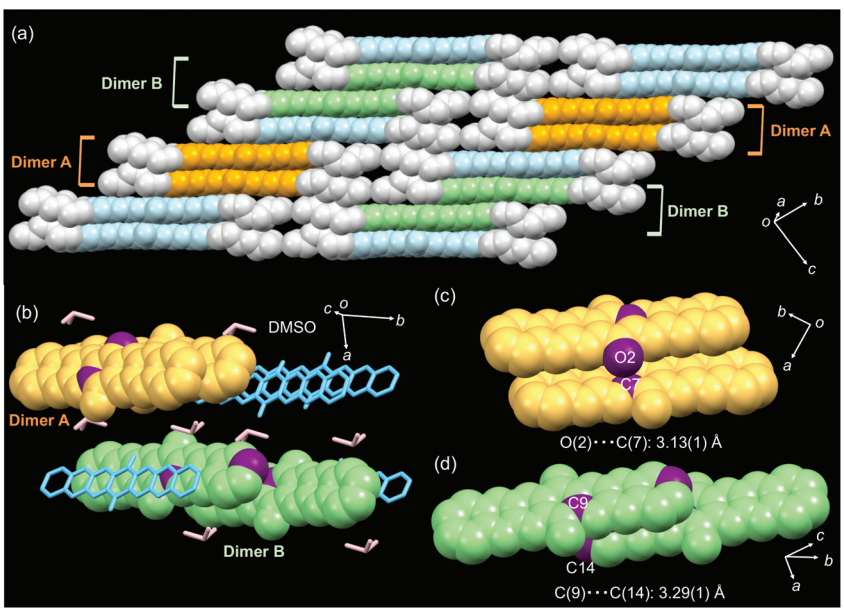

Fig. 1 Crystal structures of **C_6OAHCQ·(DMSO)**. Dimers A and B are indicated in orange and green, respectively. (a) 1D-Slipped stacking structure of **C_6OAHCQ** molecules along the *b* axis. Hydrogen atoms and DMSO molecules are omitted for clarity. (b) Dimer structures formed by **C_6OAHCQ** molecules in the 1D slipped stacking structure. Hexyloxy moieties are omitted for clarity. Structures of (c) Dimer A and (d) Dimer B. Hexyloxy moieties and DMSO molecules are omitted for clarity.

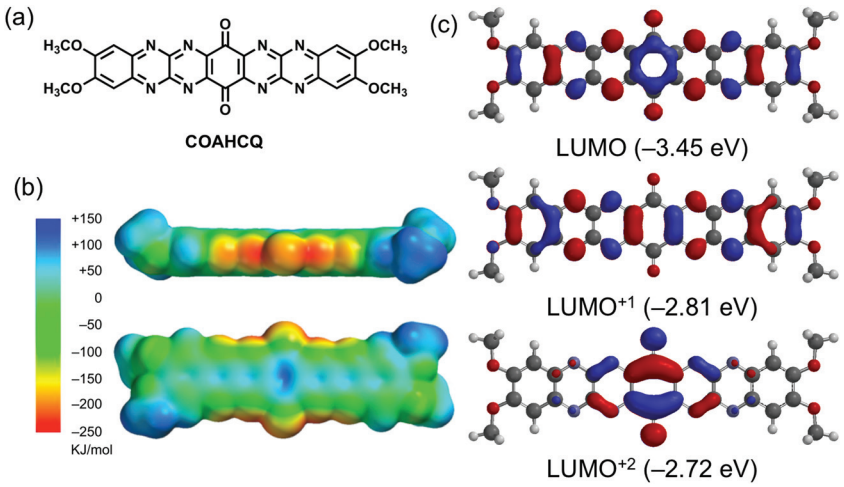

Fig. 2 (a) Molecular structure of **COAHCQ**. (b) The calculated electrostatic-potential maps and (c) LUMO, LUMO+1, and LUMO+2 of **COAHCQ** calculated with B3LYP/6-31G*.

adopts an almost planar structure. The structure of **C_6OAHCQ** shown in Fig. 1a reveals that **C_6OAHCQ** molecules stack to form a slipped one-dimensional (1D) columnar structure along the *b* axis; this column is also constructed from two types of dimer structure (Fig. 1b). Dimer A adopts a slipped stack along the short axis of the molecule, as shown in Fig. 1c, while Dimer B is aligned along the long axis of the molecule (Fig. 1d). The shortest distances between stacked molecules are as follows: O(2)···C(7) = 3.13(1) Å for Dimer A and C(9)···C(14) = 3.29(1) Å for Dimer B. Dimers A and B are alternately stacked along the **C_6OAHCQ** column, which leads to the formation of the 1D columnar structure shown in Fig. 1a. To further investigate the forces that drive packing within the **C_6OAHCQ** crystal, the electronic structure of **C_6OAHCQ** was determined by density functional theory (DFT) calculations at the B3LYP/6-31G* level of theory within the SPARTAN'08 package (Fig. 2 and S1†).[39–41] We used the tetramethoxy-substituted **COAHCQ** molecule for clarity (Fig. 2a). DFT calculations reveal that **COAHCQ** accumulates negative charge on the two carbonyl oxygen atoms of its benzoquinone framework and its eight imino-N atoms (Fig. 2b). As a result, the charge is clearly depleted from the aromatic rings substituted by the electron-withdrawing carbonyl and imino-N groups. It should be noted that the observed O(2)···C(7) distance in Dimer A is much shorter than the sum of van der Waals radii of C and O (C–O: 3.22 Å),[42,43] which indicates that electrostatic interactions operate between the negatively charged carbonyl groups or imino-N atoms (red colour) and the positively charged rings (blue colour). The shorter intermolecular distances lead to an enhanced transfer integral and more efficient electron-transport behaviour. Therefore, the flexible alkoxy chains at the terminal benzene rings impart significant advantages that improve solubility and molecular arrangements in the crystal state.

Spectroelectrochemical experiments and electrochromic behaviour

The electronic properties of **C_6OAHCQ** were evaluated by UV-vis absorption spectroscopy in the solution state. The UV-vis absorption spectrum of **C_6OAHCQ** exhibits its lowest absorption maximum at 500 nm and an absorption edge at 550 nm (Fig. 3a, black solid line); this spectrum is compared to that of **TAPQ**[34,35] (Scheme 1, Table 1), an analogue of **C_6OAHCQ**. **TAPQ** exhibits an absorption maximum at 356 nm and an absorption onset at 395 nm.[34,35] Hence, **C_6OAHCQ** exhibits an absorption maximum that is bathochromically shifted by 155 nm compared to that of **TAPQ**, which suggests that increasing the number of imino-N atoms and expanding the π-conjugated system stabilises the LUMO level of **C_6OAHCQ**, resulting in a narrower HOMO–LUMO gap compared to that of **TAPQ**. The experimental result for **C_6OAHCQ** is in good agreement with that obtained by DFT, in which the LUMO of **COAHCQ** was found to be mainly located on the carbonyl and imino-N groups of the benzoquinone framework (Fig. 2c), which indicates that the carbonyl and imino-N groups contribute to lowering the energy of the LUMO.

The redox behaviour of **C_6OAHCQ** was studied by cyclic voltammetry (CV), the results of which are shown in Fig. 3b and S2.† The cyclic voltammogram of **C_6OAHCQ** in CH_2Cl_2 solution containing $^nBu_4NPF_6$ as the electrolyte exhibits reversible two-step reduction waves at the half-wave potentials ($E_{1/2}$) of −0.55 V ($1e^-$) and −0.83 V ($1e^-$) and two-step reduction waves at −1.67 ($1e^-$) and −1.75 V ($1e^-$) *vs.* Fc^+/Fc. On the other hand, no peak was observed in an anodic potential. The number of electrons transferred from the working electrode to **C_6OAHCQ** was determined by differential pulse voltammetry (DPV) (Fig. 3b). To determine the electron-accepting moiety involved in the first consecutive two-step reduction, we resorted to DFT calculations (Fig. 2c). The LUMO, LUMO+1, and LUMO+2 orbitals are calculated to clearly reside on the benzoquinone moiety bearing the two carbonyl units, as opposed to the pyrazine moieties with the imino-N atoms (Fig. 2c), which indicates that the first consecutive two-step two-electron reductions correspond to the formation of radical-anion and dianion species on the benzoquinone moiety, respectively.

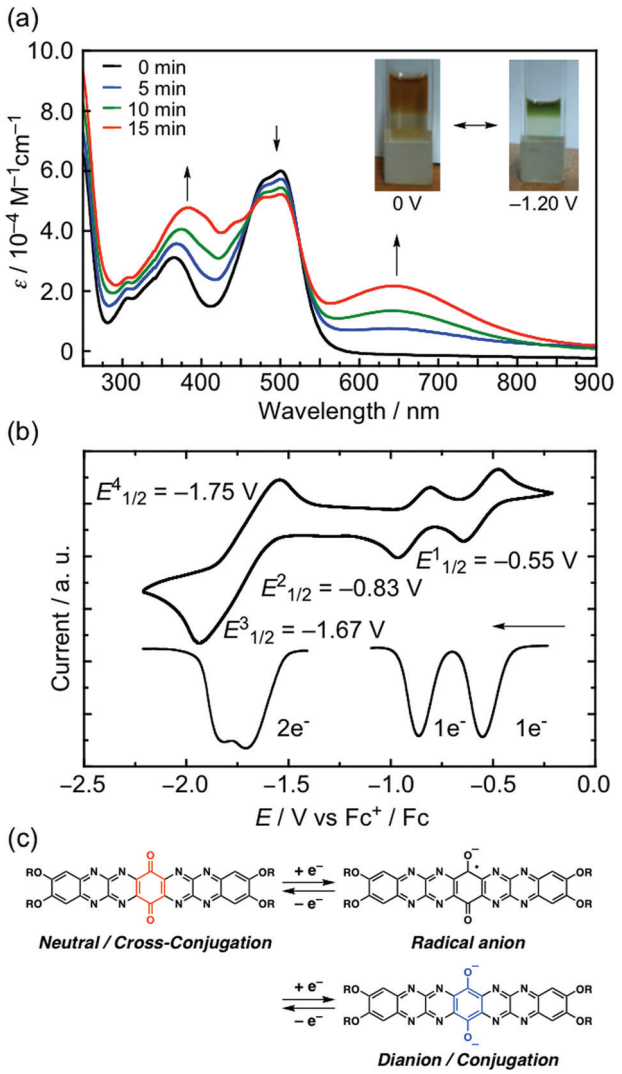

Fig. 3 (a) Time-dependent UV-vis absorption spectra of **C_6OAHCQ** at an applied voltage of −1.2 V in a 0.10 M solution of ^{n}Bu$_4$NPF$_6$ in CH_2Cl_2. The photographic images in the inset depict the electrochromic behaviour of the **C_6OAHCQ** solution: E = 0 V (left) and E = −1.2 V (light). (b) Cyclic (upper) and differential-pulse voltammograms (bottom) of 1.0 mM **C_6OAHCQ** in a 0.10 M solution of ^{n}Bu$_4$NPF$_6$ in CH_2Cl_2 at a scanning rate of 100 mV s^{-1}. (c) Depicting the structural changes undergone by **C_6OAHCQ** during the redox reaction (R = C_6H_{13}).

Successive two-step two-electron transfers at $E^3_{1/2}$ and $E^4_{1/2}$ are ascribed to two-electron reductions of the two aromatic tetraaza frameworks to form tetranion species. It should be noted that a large gap is observed between the second and the third reduction potentials ($\Delta E = E^2_{1/2} - E^3_{1/2}$), which suggests that the two-electron reduction on the benzoquinone framework delocalizes the negative charge on the molecular entity because the cross-conjugated electronic structure of neutral **C_6OAHCQ** transforms into the fully conjugated structure (Fig. 3c).[44,45] Moreover, since the obtained **C_6OAHCQ** dianion exhibits on-site coulombic repulsion, more negative potential is required in order to accept more electrons for further reduction (Fig. S7†).[46]

We next compared the electrochemical properties and energy levels of **C_6OAHCQ** with those of the **TAPQ** analogue (Table 1). The LUMO level of **C_6OAHCQ** is much lower than that of **TAPQ**, in spite of the four electron-donating alkoxy chains. This result suggests that the substitution of two electron-deficient imino-N atoms into the **TAPQ** framework is more influential than alkoxy-chain substitution. Moreover, the narrower HOMO–LUMO gap (E_g) for **C_6OAHCQ** compared to that of **TAPQ** is attributed to the expanded π-conjugated system. It should be noted that **C_6OAHCQ** can accept four electrons in the 0 to −2.20 V potential window, which is more than fullerene C_{60} could accept, a representative electron acceptor that can only accept three electrons.[47,48]

C_6OAHCQ was subjected to spectroelectrochemical experiments in the same electrolyte used for CV (Fig. 3a). A new absorption band centred at 650 nm gradually appears as the potential is made more negative (*i.e.*, from 0 to −1.20 V), and it is accompanied by a decrease in the absorption band at 500 nm and an increase and a bathochromic shift of the 370 nm band. The presence of two isosbestic points at 463 nm and 524 nm was observed, indicating that an electrochemical reaction, from the neutral to the dianionic species, occurs without decomposition or the generation of by-products. The colour of the **C_6OAHCQ** solution gradually changes from brown to green as the applied potential changes from 0 to −1.20 V; the green colour is assigned to the **C_6OAHCQ** dianion. The initial UV-vis absorption spectrum of neutral **C_6OAHCQ** can be recovered by returning the potential to 0 V in Fig. S3 and S4.† On the other hand, poor colour reversibility is revealed at applied voltages of −0.70 and −2.20 V, which is

Table 1 Electrochemical data and energy levels of **C_6OAHCQ**, **TAPQ** and C_{60}

Compound	UV-vis absorption/nm λ_{max}	Absorption edge/nm	Redox potential/*V vs.* Fc^+/Fc[a] $E^1_{1/2}$	$E^2_{1/2}$	$E^3_{1/2}$	E_{LUMO}/eV	E_{HOMO}/eV	E_g^{opt}/eV
C_6OAHCQ	304, 362, 478, 500	550	−0.55	−0.83	−1.71	−4.25[b]	−6.50[b]	2.25[b]
TAPQ[c]	300, 356	395	−1.02	—	—	−3.78	−6.92	3.15
C_{60}[d]	—	—	−0.98	−1.37	−1.87	−3.82	—	—

[a] Measured by cyclic voltammetry in a CH_2Cl_2 solution of ^{n}Bu$_4$NPF$_6$ (0.10 M). [b] E_{LUMO} is calculated from the first half-wave potential: $E_{LUMO} = -E^1_{1/2} - 4.8$ eV. E_{HOMO} is calculated by the following equation: $E_{HOMO} = E_{LUMO} - E_g^{opt}$. E_g^{opt} is estimated from the edge position of the UV-vis absorption spectrum in a CH_2Cl_2 solution: $E_g^{opt} = 1240/\lambda_{onset}$. [c] TAPQ data are taken from ref. 34 and 35. [d] C_{60} data are taken from ref. 47 and 48. Half-wave potentials are shown in the region of 0 to −2.2 V.

attributable to the lower stabilities of the monoanionic and tetraanionic species generated at those potentials, respectively (Fig. S5 and S6†). The good electrochromic reversibility exhibited by **C_6OAHCQ** between 0 V and −1.20 V strongly indicates that the generated dianionic species is more stable than the monoanionic or tetraanionic species.

Conclusions

We synthesised a novel electron-accepting N-heteroheptacenequinone **OAHCQ** derivative as a large π-conjugated framework. The **OAHCQ** derivative was composed of eight electron-deficient imino-N atoms and an electron-accepting benzoquinone. The **OAHCQ** derivative exhibited reversible four-step, four-electron reduction waves in its CV trace. The number of electrons accepted by **C_6OAHCQ** in the 0 to −2.20 V window is more than that accepted by electron-accepting fullerene C_{60}. In addition, the **OAHCQ** derivative shows electrochromism at negative voltages. Moreover, the HOMO and LUMO energy levels (E_{HOMO} and E_{LUMO}) of **C_6OAHCQ** can be approximately determined from the $E^1_{1/2}$ potentials in its cyclic voltammogram and the absorption edge of its UV-vis spectrum. The E_{LUMO} of **C_6OAHCQ**, at −4.29 eV, is comparable to that of the well-known methyl [6,6]-phenyl-C_{61}-butyrate electron acceptor (PCBM, −3.8 eV),[49] which is expected to function as an n-type semiconductor. The introduction of tetraaza units and the electron-withdrawing benzoquinone is a novel strategy for the design of high-electron-affinity molecules.

Experimental section

General methods

^{1}H and ^{13}C NMR spectra were recorded on a JEOL JNM-LA300 spectrometer. ^{1}H and ^{13}C NMR chemical shifts are referenced against tetramethylsilane (δ = 0.00) and $CDCl_3$ (δ = 77.00), respectively. FT-IR spectra were acquired with a HORIBA FREEXACT-II spectrometer. Matrix-assisted laser desorption/ionisation time-of-flight (MALDI-TOF) mass spectra were collected on a JEOL JMS-S3000 instrument using dithranol as the matrix. Elemental analyses were carried out with a PerkinElmer 2400 Series II CHNS/O analyser. Cyclic voltammetry was carried out in a 0.10 M solution of ^{n}Bu$_4$NPF$_4$ in CH_2Cl_2, with glassy-carbon working, Pt counter, and Ag/Ag$^+$ reference electrodes using an ALS CHI 600E electrochemical analyser. UV-vis absorption spectra were acquired with a JASCO V-550 UV-vis spectrometer. Spectroelectrochemical studies were conducted in a three-electrode quartz cell with the same electrolyte system as CV using the potentiostat together with a JASCO V-550 spectrometer and a PerkinElmer Lambda35 UV-vis spectrometer. During applying the voltage, Ar gas was flowed into the solution to diffuse the compounds in the cell entirely. Density functional theory (DFT) calculations were carried out using the Wavefunction SPARTAN'08 suite of programs. Ground-state geometries were optimised at the B3LYP/6-31G* level of theory.[39–41] Single-crystal X-ray diffraction data for **C_6OAHCQ·(DMSO)** were collected at 173 K on a Bruker Apex II Ultra X-ray diffractometer using Mo Kα radiation (λ = 0.71073 Å). Intensity data were processed using APEX2 software, and the structures were solved using direct methods and refined using SHELXL-2014 (full-matrix least-squares on F^2) in APEX2.[50,51] The carbon atoms in parts of one hexyloxy group (part A: C38A, C39A, and C40A; part B: C38B, C39B, and C40B) were disordered over two positions. The anisotropic displacement parameters of these atoms were restrained. Crystallographic data files are available from the Cambridge Crystallographic Data Centre (CCDC no. 1871181†).

Synthesis of C_6OAHCQ

2,3-Dihydroxy-6,7-dihexyloxyquinoxaline (4). Hydrazine monohydrate (30.0 g, 60.0 mmol) was added dropwise to a suspension of 4,5-dihexyloxy-1,2-dinitrobenzene (**5**)[37] (3.68 g, 10.0 mmol) and Pd/C (1.0 g) in dry EtOH (100 mL) at 0 °C, after which the mixture was refluxed for 24 h. The reaction mixture was filtered through Celite under Ar. After the evaporation of the solvent, the crude product and diethyl oxalate (40.0 mL, large excess) in dry EtOH (50 mL) were refluxed overnight. The reaction solution was cooled to 0 °C, which produced a white precipitate. After filtration, the product was purified by recrystallization, from $CHCl_3$/CH_3OH and dried under vacuum to afford **4** as a white solid (2.58 g, 71.2%). MALDI-TOF-MS (dithranol): m/z = 363 ([C_6ODHQ]$^+$). Anal. Calcd for [C_6ODHQ (H_2O)]: C, 64.67%, H, 8.41%, N, 7.54%; Found: C, 65.22%, H, 8.98%, N, 7.49%. ^{1}H NMR (DMSO-d_6/ppm): δ 11.66 (s, 2H), 6.71 (s, 2H), 3.87 (t, J = 4.8 Hz, 4H), 1.67 (quint, J = 4.8 Hz, 4H), 1.41 (m, 4H), 1.29 (m, 8H), 0.88 (t, J = 4.8 Hz, 6H). ^{13}C NMR (DMSO-d_6/ppm): δ 154.91, 144.90, 118.96, 101.43, 68.96, 31.02, 28.74, 25.22, 22.13, 13.91. IR (ATR/cm^{-1}): 3488, 2931, 1670, 1527, 1465, 1396, 1276, 1166, 840, 698, 582.

2,3-Dichloro-6,7-dihexyloxyquinoxaline (3). A solution of **4** (3.00 g, 14.0 mmol), $POCl_3$ (13.0 g, 140.0 mmol), and dimethylaniline (DMA, 3.5 g, 28.0 mmol) was heated at 125 °C for 24 h. After cooling to r.t., the precipitate was collected by filtration, recrystallized from $CHCl_3$/MeOH, and dried under vacuum to afford **3** as a white solid (3.17 g, 91.0%). MALDI-TOF-MS (dithranol): m/z = 399 ([C_6ODCQ]$^+$). Anal. Calcd for [C_6ODCQ]: C, 59.26%, H, 3.73%, N, 17.28%; Found: C, 59.21%, H, 3.62%, N, 17.15%, ^{1}H NMR ($CDCl_3$/ppm): δ 7.23 (s, 2H), 4.15 (t, J = 4.8 Hz, 4H), 1.90 (quint, J = 4.8 Hz, 4H), 1.51 (m, 4H), 1.36 (m, 8H), 0.92 (t, J = 4.8 Hz, 6H). ^{13}C NMR ($CDCl_3$/ppm): δ 153.60, 142.14, 137.85, 106.10, 69.32, 31.47, 28.62, 25.61, 22.54, 13.98. IR(ATR/cm^{-1}): 3060, 1558, 1535, 1471, 1305, 1201, 1157, 1111, 1000, 887, 750, 538.

2,3-Diamino-6,7-dihexyloxyquinoxaline (2). A suspension of **3** (1.00 g, 2.50 mmol) in liquid ammonia (15.0 mL) was heated at 130 °C for one week in an autoclave. After the evaporation of NH_3, the product was recrystallized from $CHCl_3$/MeOH and dried under vacuum to afford **2** as a yellow solid (0.90 g, quantitative). MALDI-TOF-MS (dithranol): m/z = 360 ([C_6ODAQ]).

Anal. Calcd for $[C_6ODAQ](MeOH)_{0.5}$: C, 65.39%, H, 9.10%, O, 14.88%; Found: C, 65.33%, H, 9.23%, O, 15.14%. ^{1}H NMR ($CDCl_3$/ppm): δ 7.01 (s, 2H), 4.48 (br, 4H), 4.06 (t, J = 8.8 Hz, 4H), 1.85 (quint, J = 8.8 Hz, 4H), 1.51 (m, 4H), 1.36 (m, 8H), 0.91 (t, J = 8.8 Hz, 6H). ^{13}C NMR ($CDCl_3$/ppm): δ 149.00, 143.05, 132.75, 106.81, 69.02, 31.58, 28.97, 25.69, 22.59, 14.01. IR (ATR/cm^{-1}): 3432, 3143, 2919, 2856, 1654, 1496, 1467, 1261, 1187, 833, 617.

2,3-Tetrahexyloxy-5,6,8,9,14,15,17,18-octaazaheptacene-7,16-quinone (C_6OAHCQ). A suspension of **2** (0.31 g, 15.0 mmol) and 5,6-dihydroxy-5-cyclohexene-1,2,3,4-tetrone dihydrate (0.15 g, 7.50 mmol) in dry AcOH (40 mL) was refluxed overnight under Ar. The crude reaction product was collected by filtration, washed with AcOH, H_2O, hexane, and EtOH, and dried under vacuum to obtain a green solid. A solution of $NaIO_4$ (1.60 g, 75.0 mmol) and tetrabutylammonium bromide (0.024 g, 0.75 mmol) in H_2O (30 mL) was added to a solution of the green solid in dry CH_2Cl_2 (30 mL) and stirred for 3 h at r.t. The reaction mixture was extracted three times with $CHCl_3$, and the combined organic layers were washed with H_2O and brine, and dried over anhydrous Na_2SO_4. After filtration and evaporation of the solvent, the product was purified by column chromatography (silica, $CHCl_3$/MeOH = 20 : 1), recrystallized from $CHCl_3$/MeOH, and dried under vacuum to afford **C_6OAHCQ** as a red solid (0.44 g, 72.1%). MALDI-TOF-MS (dithranol): m/z = 820 ([C_6OAHCQ]4H$^+$). Anal. Calcd for [C_6OAHCQ (H_2O)]: C, 66.17%, H, 7.00%, O, 13.41%; Found: C, 65.62%, H, 7.16%, O, 13.01%, ^{1}H NMR ($CDCl_3$/ppm): δ 7.46 (s, 4H), 4.35 (t, J = 8.8 Hz, 8H), 2.00 (quint, J = 8.8 Hz, 8H), 1.59 (m, 8H), 1.40 (m, 16H), 0.95 (t, J = 8.8 Hz, 12H). ^{13}C NMR ($CDCl_3$/ppm): δ 207.16, 159.01, 149.22, 145.68, 144.99, 105.55, 70.51, 31.52, 31.04, 28.58, 25.71, 22.65, 14.08. IR (ATR/cm^{-1}): 2948, 2854, 1697, 1617, 1556, 1454, 1417, 1384, 1238, 1168, 1087, 838.

Conflicts of interest

There are no conflicts to declare.

Acknowledgements

This work was supported by a Grant-in-Aid for Scientific Research on Innovative Areas of "New Polymeric Materials Based on Element-Blocks (No. 2401)" (JSPS KAKENHI grant numbers JP25102540 and JP15H00764) and for Scientific Research (C) (JSPS KAKENHI grant number 26410099) from the Ministry of Education, Culture, Sports, Science, and Technology of Japan, Shorai Foundation For Science and Technology, Oil&Fat Industry Kaikan, The Murata Science Foundation, and Young Scientists Fund for 2016 of Kagawa University Research Promotion Program (KURPP). We thank Dr A. Sonoda at Health Research Institute, National Institute of Advanced Industrial Science and Technology for help with the NMR measurements.

Notes and references

1 G. Li, K. Zheng, C. Wang, K. S. Leck, F. Hu, X. W. Sun and Q. Zhang, *ACS Appl. Mater. Interfaces*, 2013, **5**, 6458–6462.
2 J. E. Anthony, *Chem. Rev.*, 2006, **106**, 5028–5048.
3 J. Zhou, R. Tang, X. Wang, W. Zhang, X. Zhuang and F. Zhang, *J. Mater. Chem. C*, 2016, **4**, 1159–1164.
4 K. Kawaguchi, K. Nakano and K. Nozaki, *J. Org. Chem.*, 2007, **72**, 5119–5128.
5 N. Hashimoto, R. Umano, Y. Ochi, K. Shimahara, J. Nakamura, S. Mori, H. Ohta, Y. Watanabe and M. Hayashi, *J. Am. Chem. Soc.*, 2018, **140**, 2046–2049.
6 T. Nakamura, K. Suzuki and M. Yamashita, *J. Am. Chem. Soc.*, 2014, **136**, 9276–9279.
7 G. Balaji, D. I. Phua, W. L. Shim and S. Valiyaveettil, *Org. Lett.*, 2010, **12**, 232–235.
8 U. H. F. Bunz, *Acc. Chem. Res.*, 2015, **48**, 1676–1686.
9 J. Li and Q. Zhang, *ACS Appl. Mater. Interfaces*, 2015, **7**, 28049–28062.
10 U. H. F. Bunz, J. U. Engelhart, B. D. Lindner and M. Schaffroth, *Angew. Chem., Int. Ed.*, 2013, **52**, 3810–3821.
11 U. H. F. Bunz, *Chem. – Eur. J.*, 2009, **15**, 6780–6789.
12 K. Isoda, T. Abe, M. Funahashi and M. Tadokoro, *Chem. – Eur. J.*, 2014, **20**, 7232–7235.
13 K. Isoda, T. Abe and M. Tadokoro, *Chem. – Asian J.*, 2013, **8**, 2951–2954.
14 K. Isoda, M. Nakamura, T. Tatenuma, H. Ogata, T. Sugaya and M. Tadokoro, *Chem. Lett.*, 2012, **41**, 937–939.
15 G. J. Richards, J. P. Hill, N. K. Subbaiyan, F. D'Souza, P. A. Karr, M. R. J. Elsegood, S. J. Teat, T. Mori and K. Ariga, *J. Org. Chem.*, 2009, **74**, 8914–8923.
16 G. J. Richards, J. P. Hill, T. Mori and K. Ariga, *Org. Biomol. Chem.*, 2011, **9**, 5005–5017.
17 J.-i. Nishida, N. Naraso, S. Murai, E. Fujiwara, H. Tada, M. Tomura and Y. Yamashita, *Org. Lett.*, 2004, **6**, 2007–2010.
18 T. Takeda, J. y. Tsutsumi, T. Hasegawa, S.-i. Noro, T. Nakamura and T. Akutagawa, *J. Mater. Chem. C*, 2015, **3**, 3016–3022.
19 Y. Miura and N. Yoshioka, *Chem. – Asian J.*, 2018, **13**, 1683–1687.
20 Z. Liang, Q. Tang, R. Mao, D. Liu, J. Xu and Q. Miao, *Adv. Mater.*, 2011, **23**, 5514–5518.
21 B. D. Lindner, J. U. Engelhart, O. Tverskoy, A. L. Appleton, F. Rominger, A. Peters, H. J. Himmel and U. H. Bunz, *Angew. Chem., Int. Ed.*, 2011, **50**, 8588–8591.
22 A. Maliakal, K. Raghavachari, H. Katz, E. Chandross and T. Siegrist, *Chem. Mater.*, 2004, **16**, 4980–4986.
23 Q. Tang, D. Zhang, S. Wang, N. Ke, J. Xu, J. C. Yu and Q. Miao, *Chem. Mater.*, 2009, **21**, 1400–1405.
24 J. U. Engelhart, B. D. Lindner, O. Tverskoy, M. Schaffroth, F. Rominger and U. H. Bunz, *J. Org. Chem.*, 2013, **78**, 1249–1253.
25 S. Miao, S. M. Brombosz, P. V. Schleyer, J. I. Wu, S. Barlow, S. R. Marder, K. I. Hardcastle and U. H. Bunz, *J. Am. Chem. Soc.*, 2008, **130**, 7339–7344.

26 H.-Y. Chen and I. Chao, *ChemPhysChem*, 2006, **7**, 2003–2007.
27 M. Winkler and K. N. Houk, *J. Am. Chem. Soc.*, 2007, **129**, 1805–1815.
28 Y. Ding, Y. Li and G. Yu, *Chem*, 2016, **1**, 790–801.
29 B. Rausch, M. D. Symes and L. Cronin, *J. Am. Chem. Soc.*, 2013, **135**, 13656–13659.
30 R. I. Pinhassi, D. Kallmann, G. Saper, H. Dotan, A. Linkov, A. Kay, V. Liveanu, G. Schuster, N. Adir and A. Rothschild, *Nat. Commun.*, 2016, **7**, 12552.
31 F. Asghari-Haji, K. Rad-Moghadam and N. O. Mahmoodi, *RSC Adv.*, 2016, **6**, 27388–27394.
32 Z. Liang, Q. Tang, J. Xu and Q. Miao, *Adv. Mater.*, 2011, **23**, 1535–1539.
33 Q. Miao, *Adv. Mater.*, 2014, **26**, 5541–5549.
34 Q. Tang, Z. Liang, J. Liu, J. Xu and Q. Miao, *Chem. Commun.*, 2010, **46**, 2977–2979.
35 Z. Liang, Q. Tang, J. Liu, J. Li, F. Yan and Q. Miao, *Chem. Mater.*, 2010, **22**, 6438–6443.
36 Q. Miao, *Synlett*, 2012, **23**, 326–336.
37 M. J. Howard, F. R. Heirtzler and S. I. G. Dias, *J. Org. Chem.*, 2008, **73**, 2548–2553.
38 M. Wang, Y. Li, H. Tong, Y. Cheng, L. Wang, X. Jing and F. Wang, *Org. Lett.*, 2011, **13**, 4378–4381.
39 P. C. Hariharan and J. A. Pople, *Chem. Phys. Lett.*, 1972, **16**, 217–219.
40 C. Lee, W. Yang and R. G. Parr, *Phys. Rev. B: Condens. Matter Mater. Phys.*, 1988, **37**, 785–789.
41 P. C. Hariharan and J. A. Pople, *Theor. Chim. Acta*, 1973, **28**, 213–222.
42 R. S. Rowland and R. Taylor, *J. Phys. Chem.*, 1996, **100**, 7384.
43 A. Bondi, *J. Phys. Chem.*, 1964, **68**, 441–451.
44 M. Baghernejad, X. Zhao, K. Baruël Ørnsø, M. Füeg, P. Moreno-García, A. V. Rudnev, V. Kaliginedi, S. Vesztergom, C. Huang, W. Hong, P. Broekmann, T. Wandlowski, K. S. Thygesen and M. R. Bryce, *J. Am. Chem. Soc.*, 2014, **136**, 17922–17925.
45 M. Gholami and R. R. Tykwinski, *Chem. Rev.*, 2006, **106**, 4997–5027.
46 H. Usta, A. Facchetti and T. J. Marks, *Org. Lett.*, 2008, **10**, 1385–1388.
47 L. Echegoyen and L. E. Echegoyen, *Acc. Chem. Res.*, 1998, **31**, 593–601.
48 Q. Xie, E. Perez-Cordero and L. Echegoyen, *J. Am. Chem. Soc.*, 1992, **114**, 3978–3980.
49 J. C. Hummelen, B. W. Knight, F. LePeq, F. Wudl, J. Yao and C. L. Wilkins, *J. Org. Chem.*, 1995, **60**, 532–538.
50 G. M. Sheldrick, *Acta Crystallogr., Sect. C: Struct. Chem.*, 2015, **71**, 3–8.
51 G. M. Sheldrick, *Acta Crystallogr., Sect. A: Found. Adv.*, 2015, **71**, 3–8.